Available online at www.sciencedirect.com
ScienceDirect
Journal of Photochemistry and Photobiology A: Chemistry 187 (2007) 233–241
Journal of Photochemistry and Photobiology A:Chemistry
www.elsevier.com/locate/jphotochem

Theoretical studies of charge-transfer complexes of I_2 with pyrazoles, and implications on the dye-sensitized solar cell performance

Hitoshi Kusama *, Hideki Sugihara

Energy Technology Research Institute, National Institute of Advanced Industrial Science and Technology (AIST), AIST Tsukuba Central 5, 1-1-1 Higashi, Tsukuba, Ibaraki 305-8565, Japan

Received 20 July 2006; accepted 11 October 2006
Available online 10 November 2006

Abstract

The charge-transfer 1:1 n–σ^* complexation between pyrazole derivatives and I_2 was theoretically investigated by the ab initio molecular orbital (MO) method at the second-order Møller–Plesset (MP2, full)/LANL2DZ* level. The nitrogen atom at position 2 in the pyrazole ring and the amino nitrogen atom of the substituent were preferred over the other n-donor sites of the substituents as binding sites for I_2 molecules. By comparing pyrazoles complexes binding to I_2 via the nitrogen atom at position 2 in the pyrazole ring, it was determined that the more electron donicity the substituent has at positions 3 and 5 in the pyrazole ring, the more stable the intermolecular charge-transfer complex formed. However, pyrazoles with an electron-accepting substituent at position 4 formed less favorable complexes with I_2 even if they were substituted by electron-donating groups at positions 3 and/or 5. These pyrazoles were also examined as additives in an I^-/I_3^- electrolyte solution in a Ru(II) bipyridine dye-sensitized solar cell, and the resultant open-circuit photovoltage (V_{oc}) values were correlated with the intermolecular charge-transfer properties determined by theoretical calculations. The optimized geometries, Mulliken population analyses, and natural bond orbital (NBO) analyses indicated that a V_{oc} is higher when the I_2 and pyrazoles form a more favorable intermolecular charge-transfer complex in the I^-/I_3^- redox electrolytic solution of dye-sensitized solar cell. The V_{oc} enhancing mechanism by the pyrazoles–I_2 complexation is discussed.

Keywords: Ab initio MO calculation; Charge-transfer complex; Iodine; Pyrazoles; Dye-sensitized solar cell

1. Introduction

A typical dye-sensitized solar cell consists of a nanocrystalline TiO_2 film photoelectrode covered with a monolayer of a sensitizing dye such as a Ru(II) bipyridine complex, a redox electrolyte like I^-/I_3^-, and a counter electrode such as Pt. This type of solar cell has been intensively studied since Grätzel and O'Reganoulos reported a very high solar energy conversion efficiency (η) [1]. One method to improve solar cell performance is to add organic compounds to the electrolytic solution. For example, Frank and co-workers have added ammonia and pyridine derivatives such as 4-*t*-butylpyridine and have reported that these additives drastically enhance both the V_{oc} and η [2,3]. Boschloo et al. have reported that adding 1-methylbenzimidazole increases the V_{oc} of the cell [4,5]. Based on these findings, we have reported in a previous paper an experimental study on the influence of nitrogen-containing heterocyclic additives to an I^-/I_3^- redox electrolyte in acetonitrile on dye-sensitized TiO_2 solar cell performance. Consequently, it was determined that pyrazole improves the V_{oc}, and shows the highest η value among the tested five-membered additives [6].

Moreover, Shi et al. have recently reported that 4-*t*-butylpyridine forms 4-*t*-butylpyridine-I_2 with iodine, which removes iodine adsorbed on the dye and improves the V_{oc} of dye-sensitized solar cell [7]. This chemical reaction can be written as:

$$\text{4-}t\text{-butylpyridine} + I_2 \rightarrow \text{4-}t\text{-butylpyridine-}I_2. \quad (1)$$

The molecular complexes formed by this type of interaction are known as charge-transfer (or electron donor–acceptor) molecular complexes. The electron transfer from the nonbonding molecular orbital n of the nitrogen atom in the pyridine ring to the antibonding molecular orbital σ^* of I_2 forms a n–σ^* complex. Although complexes of I_2 with pyridine have been intensely investigated [8–15], there are few experimental studies on pyrazole complexes [16,17]. Moreover, publications on the

* Corresponding author. Tel.: +81 29 861 4867; fax: +81 29 861 6771.
E-mail address: h.kusama@aist.go.jp (H. Kusama).

1010-6030/$ – see front matter © 2006 Elsevier B.V. All rights reserved.
doi:10.1016/j.jphotochem.2006.10.022

geometric fields, such as the N···I bond length are unavailable in the literature. However, analysis of complexation of I_2 with pyrazoles is possible. To aid in the understanding of intermolecular charge-transfer complexation, numerous computational simulations have been attempted on I_2 with amines [18–20] and pyridines [18,21,22]. However, to the best of our knowledge, theoretical calculations on intermolecular complexes of I_2 with pyrazoles have yet to be reported. This study investigates the charge-transfer 1:1 n–σ^* complexes between I_2 and 15 types of pyrazoles by ab initio MO method with optimized geometries. These effects of pyrazoles additives in an I^-/I_3^- electrolytic solution on Ru(II) bipyridine dye-sensitized solar cell performance are also examined. The present study aims to theoretically identify the interaction properties of pyrazoles–I_2 and to confirm the correlation between the V_{oc} of the solar cell and the intermolecular charge-transfer properties.

2. Calculation methods

All ab initio MO calculations were performed using the Gaussian 03W Revision D.01 program [23] with GaussView 3.09 Software [24] on personal computers. The monomer and complex geometries were fully optimized at the MP2(full) levels. For all systems, a LANL2DZ* basis set, which includes an effective core potential (ECP) for all atoms except for the first row [25], was used. Hay and Wadt proposed the ECP used [26–28] in which the iodine incorporates the mass velocity and Darwin relativistic effects. The LANL2DZ basis set corresponds to a Dunning/Huzinaga full double-ζ basis (D95) [29] for first-row elements and an ECP plus double-ζ basis for the iodine atoms [30]. This basis set was augmented with one set of six d polarization function (LANL2DZ*) with the following exponents: $\alpha_C = \alpha_N = \alpha_O = 0.8$, $\alpha_S = 0.65$, $\alpha_{Br} = 0.39$ and $\alpha_I = 0.29$ [31,32]. Recently, this basis set was shown to yield reasonable results for charge-transfer complexes of I_2 with pyridine [22], thiocarbonyl derivatives [33], and lactams [34]. To correct for the intermolecular bond energy, the counterpoise (CP) correction was incorporated from the basis set superposition error (BSSE) using Boys and Bernardi procedure [35,36]. The harmonic vibrational frequencies confirmed that the optimized structures correspond to real minima on the potential energy surface [37].

To understand the nature and magnitude of the intermolecular interactions, NBO analysis [30,38] was conducted on the optimized geometries using the NBO 3.1 program [39], which is included in the Gaussian package program.

3. Experimental

Preparation of dye-sensitized solar cell and its photovoltaic characterization was conducted as previously described [6]. A sandwich-type solar cell consisted of a nanocrystalline TiO_2 photoelectrode (1.5×10^{-5} m thick) with bis(tetrabutylammonium)*cis*-bis(thiocyanato)bis(2,2′-bipyridine-4-carboxylic acid,4′-carboxylate)ruthenium(II) dye (N719), a 2.5×10^{-5} m thick Lumirror spacer film, and a counter electrode, which was a Pt sputtered FTO conducting glass. The electrolytic solution, which was composed of 0.5 mol/dm^3 of a pyrazole additive, 0.6 mol/dm^3 1,2-dimethyl-3-propylimidazolium iodide, 0.1 mol/dm^3 LiI, 0.05 mol/dm^3 I_2, and acetonitrile as the solvent, was injected into the space between the two electrodes. The solar cell performance was measured under simulated solar light (AM 1.5, 100 mW/cm^2). The photovoltage was measured using a digital source meter and a data acquisition system. The apparent cell area of the TiO_2 photoelectrode was 0.25 cm^2 (0.5 cm × 0.5 cm).

4. Results and discussion

4.1. Theoretical calculations of isolated molecules and complexes

Table 1 lists select characteristic results for the optimized geometries of the isolated I_2 and pyrazoles molecules.

Table 1
Calculated energies of the isolated molecules, and energies of the HOMO and LUMO levels

No.	Compound	Energy (a.u.)	HOMO (a.u.)	LUMO (a.u.)
	I_2	−22.53646	−0.36123	−0.02495
1	3-Methylpyrazole	−264.69844	−0.33882	0.15872
2	3,5-Dimethylpyarzole	−303.87251	−0.32559	0.16756
3	3,5-Diisopropylpyrazole	−460.55012	−0.32083	0.16685
4	4-Bromo-3-methylpyrazole	−277.17183	−0.33508	0.17577
5	3,5-Dimethyl-4-iodopyrazole	−314.55818	−0.31705	0.12778
6	3-Aminopyrazole	−280.72613	−0.31998	0.15819
7	3-Amino-5-methylpyrazole	−319.90024	−0.31457	0.16887
8	3-Amino-5-*t*-butylpyrazole	−437.41175	−0.31243	0.16871
9	3-Amino-4-phenylpyrazole	−511.04934	−0.32671	0.11253
10	5-Amino-3-phenylpyrazole	−511.04683	−0.29687	0.10715
11	3-Amino-4-bromopyrazole	−293.19885	−0.32448	0.17464
12	3-Amino-4-cyanopyrazole	−372.75003	−0.34497	0.10726
13	3-Amino-4-cyano-5-methylthiopyrazole	−421.95533	−0.34165	0.09130
14(*sp*)	5-Amino-3-(2-thienyl)pyrazole	−443.90962	−0.28750	0.09665
14(*ap*)	5-Amino-3-(2-thienyl)pyrazole	−443.90892	−0.28749	0.09722
15(*sp*)	3-Amino-5-(2-furyl)pyrazole	−508.91426	−0.32615	0.09088
15(*ap*)	3-Amino-5-(2-furyl)pyrazole	−508.91219	−0.32694	0.09722

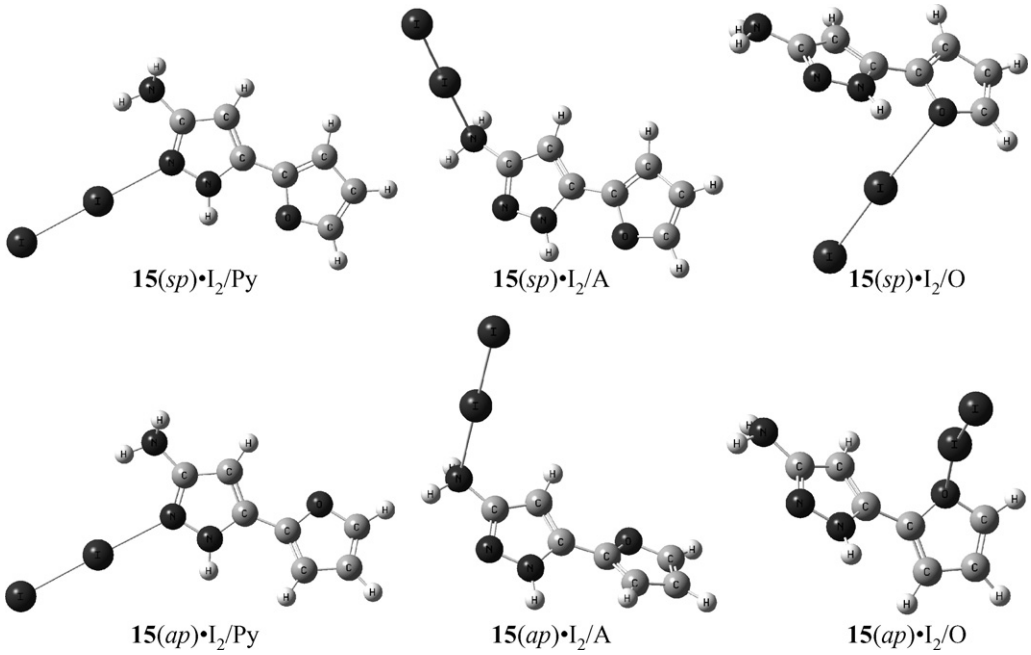

Fig. 1. Optimized geometries of **15**·I_2 complexes.

For 5-amino-3-(2-thienyl)pyrazole (**14**) and 3-amino-5-(2-furyl)pyrazole (**15**), there are two conformers, denoted *sp* and *ap*, which have the nitrogen atom at position 2 in the pyrazole ring and the sulfur or oxygen atom in the thiophene or furan ring of substituent oriented synperiplanar and antiperiplanar, respectively.

Except for compounds **1**–**5**, more than one constitutional isomer can be formed because there is more than one potential *n*-donor site in the tested pyrazoles: the nitrogen atom at position 2 in the pyrazole ring (Py), the amino nitrogen atom (A), cyano nitrogen atom (CN), methylthio sulfur atom (S), sulfur atom in the thiophene ring and oxygen atom in the furan ring (O). However, compounds **14**(*sp*) and **14**(*ap*) did not have a stable I_2 complex structure binding via the sulfur atom in the thiophene ring of the substituent. Fig. 1 illustrates the optimized geometries using compound **15**, which has six constitutional isomers, as an example.

Table 2 presents selected results from the optimized geometries for the pyrazoles–I_2 complexes. The lengthened intramolecular I–I bonds, which are observed for all complexes, indicate that the I_2 monomer bond is weakened in the complex structures. The forming intermolecular σ-bonds, N···I, O···I, and S···I are stronger than the net van der Waals radii (3.53, 3.40 and 3.78 Å) of the binding atoms, but weaker than the net covalent radii (2.03, 1.99 and 2.37 Å). These findings provide initial evidence that all the tested pyrazoles form intermolecular charge-transfer complexes with I_2. The longer the I–I bond length and the shorter the R···I (R = N, O, S) one, the more favorable complexation is. Judging from the I–I bond length, the nitrogen atom at position 2 in the pyrazole ring and the amino nitrogen atom of the substituent are stronger binding sites for I_2 molecules than the other *n*-donor sites of the substituents. All of the R···I–I bond angles are approximately linear.

Table 2
Selected bond lengths (Å) and angles (°) of I_2 and the complexes

Species	I—I	R···I	R···I—I
I_2	2.694		
1·I_2/Py	2.748	2.651	176.78
2·I_2/Py	2.753	2.629	176.75
3·I_2/Py	2.756	2.615	176.92
4·I_2/Py	2.740	2.688	176.44
5·I_2/Py	2.745	2.662	176.44
6·I_2/Py	2.750	2.636	178.80
6·I_2/A	2.753	2.695	179.43
7·I_2/Py	2.755	2.613	178.69
7·I_2/A	2.758	2.678	179.24
8·I_2/Py	2.757	2.607	178.64
8·I_2/A	2.759	2.670	179.02
9·I_2/Py	2.751	2.633	178.88
9·I_2/A	2.756	2.688	179.97
10·I_2/Py	2.744	2.671	175.67
10·I_2/A	2.736	2.783	179.84
11·I_2/Py	2.742	2.669	178.69
11·I_2/A	2.745	2.737	179.53
12·I_2/Py	2.732	2.721	178.80
12·I_2/A	2.733	2.797	178.78
12·I_2/CN	2.711	2.876	179.60
13·I_2/Py	2.733	2.719	178.77
13·I_2/A	2.732	2.796	178.83
13·I_2/CN	2.711	2.874	179.00
13·I_2/S	2.715	3.330	178.99
14(*sp*)·I_2/Py	2.738	2.702	174.19
14(*sp*)·I_2/A	2.735	2.790	179.81
14(*ap*)·I_2/Py	2.743	2.672	175.61
14(*ap*)·I_2/A	2.735	2.788	179.99
15(*sp*)·I_2/Py	2.750	2.637	179.01
15(*sp*)·I_2/A	2.753	2.694	178.90
15(*sp*)·I_2/O	2.701	3.075	177.46
15(*ap*)·I_2/Py	2.750	2.637	178.75
15(*ap*)·I_2/A	2.752	2.697	179.51
15(*ap*)·I_2/O	2.702	3.116	171.16

Table 3
Total energies (E_{tot}) of the title species, complexation energies (ΔE_b), BSSE and the complexation energies after the CP correction (ΔE_b^{CP})

Species	E_{tot} (a.u.)	ΔE_b (kcal mol^{-1})	BSSE (kcal mol^{-1})	ΔE_b^{CP} (kcal mol^{-1})
1·I_2/Py	−287.24725	10.64	2.89	7.75
2·I_2/Py	−326.42212	11.29	3.03	8.26
3·I_2/Py	−483.10049	11.87	3.14	8.73
4·I_2/Py	−299.71930	9.58	2.66	6.91
5·I_2/Py	−337.10650	10.27	2.83	7.44
6·I_2/Py	−303.27470	10.56	2.96	7.60
6·I_2/A	−303.27538	10.39	2.36	8.03
7·I_2/Py	−342.44961	11.21	3.11	8.11
7·I_2/A	−342.45017	10.92	2.47	8.45
8·I_2/Py	−459.96137	11.42	3.15	8.26
8·I_2/A	−459.96200	11.20	2.55	8.65
9·I_2/Py	−533.59797	10.60	2.96	7.64
9·I_2/A	−533.59825	10.50	2.69	7.81
10·I_2/Py	−533.59529	10.51	2.98	7.53
10·I_2/A	−533.59296	8.26	2.19	6.07
11·I_2/Py	−315.74630	9.64	2.74	6.90
11·I_2/A	−315.74665	9.38	2.26	7.12
12·I_2/Py	−395.29597	8.43	2.49	5.95
12·I_2/A	−395.29577	7.80	1.98	5.82
12·I_2/CN	−395.29364	6.33	1.84	4.49
13·I_2/Py	−444.50127	8.46	2.51	5.95
13·I_2/A	−444.50099	7.82	2.05	5.78
13·I_2/CN	−444.49896	6.33	1.83	4.50
13·I_2/S	−444.49735	5.17	1.68	3.50
14(*sp*)·I_2/Py	−466.46148	12.37	2.70	9.67
14(*sp*)·I_2/A	−466.45977	10.75	2.16	8.59
14(*ap*)·I_2/Py	−466.46164	13.16	2.96	10.20
14(*ap*)·I_2/A	−466.45935	10.94	2.18	8.77
15(*sp*)·I_2/Py	−531.46278	10.52	2.95	7.57
15(*sp*)·I_2/A	−531.46346	10.40	2.41	7.99
15(*sp*)·I_2/O	−531.45484	4.10	1.51	2.59
15(*ap*)·I_2/Py	−531.46068	10.50	2.95	7.55
15(*ap*)·I_2/A	−531.46135	10.35	2.38	7.97
15(*ap*)·I_2/O	−531.45406	4.86	1.47	3.39

Table 3 lists the total energy of the complex (E_{tot}) and the intermolecular bond energy (ΔE_b). ΔE_b is due to the charge redistribution during intermolecular bonding of the donor and acceptor and can be derived as follows:

$$\Delta E_b = E(I_2) + E(\text{pyrazoles}) - E_{tot}, \quad (2)$$

where $E(I_2)$ and E(pyrazoles) are the energies of the I_2 and pyrazoles monomers, respectively (see Table 1) [20]. Table 3 also presents the calculated BSSE and the CP-corrected ΔE_b (ΔE_b^{CP}) values. It is noteworthy that the BSSE is always large (1.47–3.15 kcal mol^{-1}) and cannot be neglected [33,40]. ΔE_b^{CP} is larger when the donor and acceptor form a more stable complex. Thus, ΔE_b^{CP} indicates that the nitrogen atom at position 2 in the pyrazole ring and the amino nitrogen atom of the substituent are more favorable binding sites for I_2 molecules than the other *n*-donor sites of the substituents.

Table 4 lists the Mulliken population analysis and NBO analysis for the complexes. To complete the span of the valence space in the NBO analysis [39], each valence bonding NBO (σ_{AB}) must be paired with the corresponding valence antibonding NBO (σ^*_{AB}):

$$\sigma^*_{AB} = c_A h_A - c_B h_B. \quad (3)$$

Namely, the 'Lewis'-type (donor) NBOs are complemented by the 'non-Lewis'-type (acceptor) NBOs that are formally empty in an ideal Lewis structure picture. The general transformation to NBOs leads to unoccupied orbitals in the formal Lewis structure. Consequently, the filled NBOs of the natural Lewis structure accurately describe the covalency effects in these molecules. Because non-covalent delocalization effects are associated with $\sigma \rightarrow \sigma^*$ interactions between the filled (donor) and unfilled (acceptor) orbitals, these delocalization effects are described as 'donor–acceptor', charge transfer, or generalized 'Lewis base–Lewis acid'-type interactions. The antibonds represent the unused valence-shell capacity and spanning portions of the atomic valence space, which are formally unsaturated by covalent bond formation. Weak occupancies of the valence antibonds indicate irreducible departures from an ideal localized Lewis picture, i.e. true 'delocalization effects'.

Therefore, the donor–acceptor (bond–antibond) interactions in the NBO analysis are considered by examining all possible interactions between the 'filled' (donor) Lewis-type NBOs and the 'empty' (acceptor) non-Lewis NBOs. Then their energies are estimated by second-order perturbation theory. These interactions (or energetic stabilizations) are referred to as 'delocalization' corrections to the 0th-order natural Lewis

Table 4
The results of Mulliken population analysis and NBO analysis of the title species

Species	q_{CT}		Occupancy			$E^{(2)}$ (kcal mol^{-1})	
	Mulliken	NBO	σ^*(I—I)	n_σ(N, O, S)	n_π(O, S)	n_σ(N, O, S), σ^*(I—I)	n_π(O, S), σ^*(I—I)
1·I_2/Py	0.074	0.061	0.072	1.891		23.71	
2·I_2/Py	0.082	0.068	0.078	1.885		25.83	
3·I_2/Py	0.086	0.071	0.082	1.879		27.20	
4·I_2/Py	0.063	0.051	0.062	1.899		20.39	
5·I_2/Py	0.070	0.058	0.068	1.891		22.54	
6·I_2/Py	0.078	0.066	0.077	1.883		25.62	
6·I_2/A	0.076	0.069	0.074	1.869		23.08	
7·I_2/Py	0.086	0.073	0.084	1.877		27.92	
7·I_2/A	0.080	0.074	0.078	1.866		24.46	
8·I_2/Py	0.088	0.075	0.086	1.874		28.69	
8·I_2/A	0.083	0.076	0.081	1.864		25.15	
9·I_2/Py	0.078	0.066	0.078	1.883		25.78	
9·I_2/A	0.076	0.069	0.076	1.861		23.31	
10·I_2/Py	0.069	0.055	0.067	1.896		21.70	
10·I_2/A	0.051	0.049	0.057	1.908		17.77	
11·I_2/Py	0.068	0.057	0.068	1.891		22.41	
11·I_2/A	0.064	0.059	0.063	1.868		19.34	
12·I_2/Py	0.056	0.046	0.056	1.901		18.61	
12·I_2/A	0.049	0.045	0.051	1.870		15.50	
12·I_2/CN	0.036	0.016	0.026	1.951		9.81	
13·I_2/Py	0.056	0.046	0.057	1.900		18.63	
13·I_2/A	0.049	0.045	0.050	1.870		15.43	
13·I_2/CN	0.036	0.016	0.026	1.951		9.85	
13·I_2/S	0.035	0.039	0.041	1.971	1.881	1.17	9.72
14(*sp*)·I_2/Py	0.060	0.048	0.059	1.903		19.31	
14(*sp*)·I_2/A	0.049	0.047	0.056	1.909		17.28	
14(*ap*)·I_2/Py	0.068	0.054	0.065	1.897		21.58	
14(*ap*)·I_2/A	0.049	0.048	0.056	1.909		17.44	
15(*sp*)·I_2/Py	0.078	0.066	0.077	1.883		25.59	
15(*sp*)·I_2/A	0.076	0.069	0.075	1.869		23.13	
15(*sp*)·I_2/O	0.012	0.004	0.010	1.974	1.791	1.40	1.46
15(*ap*)·I_2/Py	0.078	0.066	0.077	1.883		25.51	
15(*ap*)·I_2/A	0.075	0.069	0.073	1.868		22.77	
15(*ap*)·I_2/O	0.010	0.004	0.009	1.974	1.782	1.27	1.15

structure. For each donor NBO (*i*) and acceptor NBO (*j*), the stabilization energy $E^{(2)}$, which is associated with the $i \rightarrow j$ delocalization, is explicitly estimated by the following equation:

$$E^{(2)} = \Delta E_{ij} = q_i \times \frac{F^2(i,\ j)}{\varepsilon_j - \varepsilon_i}, \quad (4)$$

where q_i is the *i*th donor orbital occupancy; ε_i and ε_j the diagonal elements (orbital energies), and $F(i,j)$ is the off-diagonal element associated with the NBO Fock matrix. Hence, consideration of the valence antibond (σ^*) leads to a far-reaching extension of the elementary Lewis structure concept and achieves a delocalization correction using simple NBO perturbative estimates and Eq. (4) [41].

The net charge transferred from the donor to the acceptor (q_{CT}) [22] determined by Mulliken population analysis is somewhat larger than that from the NBO one, as shown in Table 4, However, the Mulliken population analysis and NBO one have the same relative order for the complex series. The occupancy values of the oxygen and sulfur lone pairs for **13**·I_2/S, **15**(*sp*)·I_2/O and **15**(*ap*)·I_2/O indicate that the principal donor orbital of these complexes corresponds to a π type orbital. Except for **13**·I_2/S, **15**(*sp*)·I_2/O and **15**(*ap*)·I_2/O, the value of q_{CT} in the complex series gradually increases, while the donor decreases the n_σ(N) occupancy and the acceptor increases σ^*(I–I) one. The $E^{(2)}$ value for the n_σ(N) and σ^*(I–I) interaction also increases with q_{CT}. Mulliken population analysis and NBO analysis also demonstrate that the nitrogen atom at position 2 in the pyrazole ring and the amino nitrogen atom of the substituent are stronger binding sites for I_2 molecules than other *n*-donor sites of the substituents.

Comparing complexes Py indicates that the more electron donicity the substituent at positions 3 and 5 in the pyrazole ring has, the more favorable the intermolecular charge-transfer complex. However, pyrazoles with an electron-accepting substituent at position 4 form less stable complexes with I_2 even if they are substituted by electron-donating groups at positions 3 and/or 5. Compound **9** complexes more favorably with I_2 than compound **10** because the substituents in **10** have more electronic effect and steric hindrance. Conformers **14**(*ap*) and **15**(*sp*) preferably form complexes than **14**(*sp*) and **15**(*ap*), respectively.

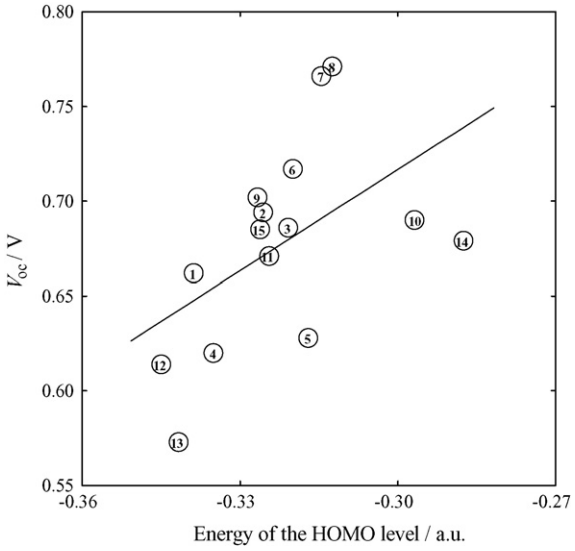

Fig. 2. Correlation between the V_{oc} of the cell and the energy of the HOMO level for the isolated pyrazoles molecules. Table 1 defines the number of each pyrazole.

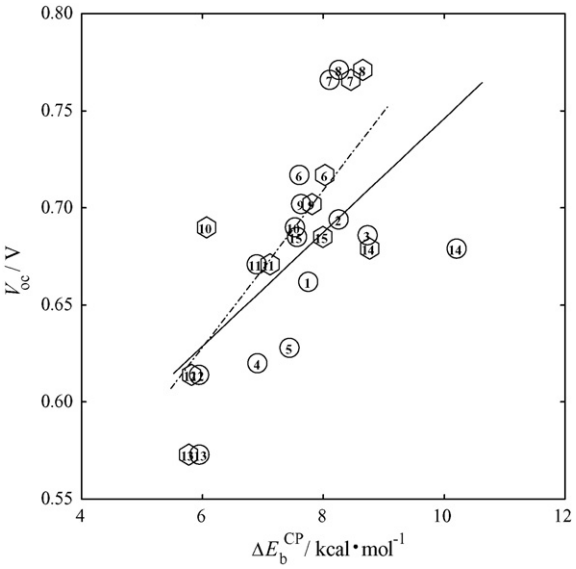

Fig. 4. Correlation between the V_{oc} of the cell and the CP-corrected intermolecular bond energy (ΔE_b^{CP}). (◯) complexes Py, (⬡) complexes A. Table 1 defines the number of each pyrazole.

4.2. Correlations between V_{oc} and theoretical calculations

Comparing the V_{oc} value of dye-sensitized solar cell with the calculated pyrazole monomer properties, the V_{oc} is correlated to the energy of the HOMO level listed in Fig. 2. The V_{oc} increases as the energy of the HOMO level increases and becomes closer to the LUMO level of I_2 molecule (−0.02495 a.u.). The correlation coefficient is 0.519. The theory of intermolecular charge-transfer complexation is explained by the interaction between the HOMO of the donors and the LUMO of the acceptors [42]. The greater the overlap and/or the smaller energy difference of the HOMO of the donors and the LUMO of acceptors, the greater the stabilization energy Δ, which corresponds to the $E^{(2)}$ for n and σ^*(I–I) interaction in Table 4 [30], and the greater the extent of mixing, which causes a greater charge transfer from the donor to the acceptor. Therefore, the correlation in Fig. 2 strongly implies that a higher V_{oc} occurs when the energy of the pyrazole HOMO level is close to the energy of the I_2 LUMO level because a more efficient charge-transfer complex is formed.

As mentioned in Section 4.1, the nitrogen atom at position 2 in the pyrazole ring and the amino nitrogen atom of the substituent are preferred over other *n*-donor sites of the substituents such as the cyano nitrogen atom, methylthio sulfur atom, sulfur atom in the thiophene ring and oxygen atom in the furan ring as binding sites for I_2 molecules. Therefore, we compared the V_{oc} values with the calculated properties of pyrazole–I_2 complexes only via binding the nitrogen atom at position 2 in the pyrazole ring (complexes Py) and the amino nitrogen atom of the substituent (complexes A). Moreover, for conformers **14** and **15**, **14**(*ap*) and **15**(*sp*) were only compared because they are more

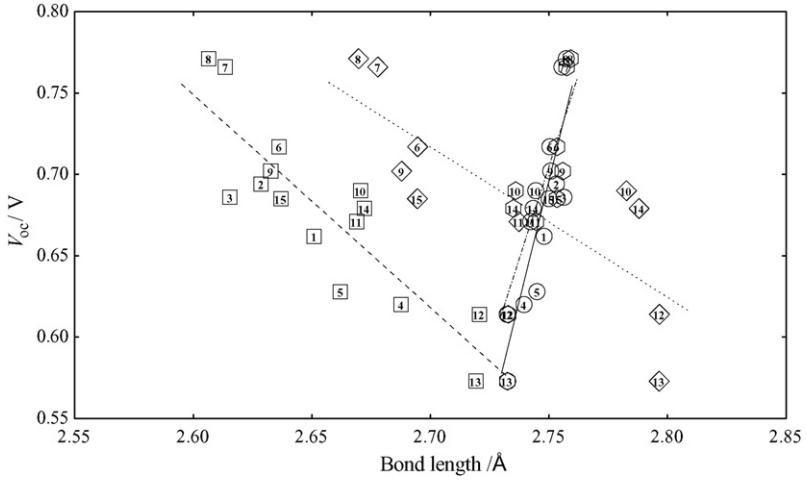

Fig. 3. Correlation between the V_{oc} of the cell and the bond length of the pyrazole–I_2 complexes. (◯) Intramolecular I—I bond length of complexes Py, (⬡) intramolecular I—I bond length of complexes A, (□) intermolecular N···I bond length of complexes Py, (◇) intermolecular N···I bond length of complexes A. Table 1 defines the number of each pyrazole.

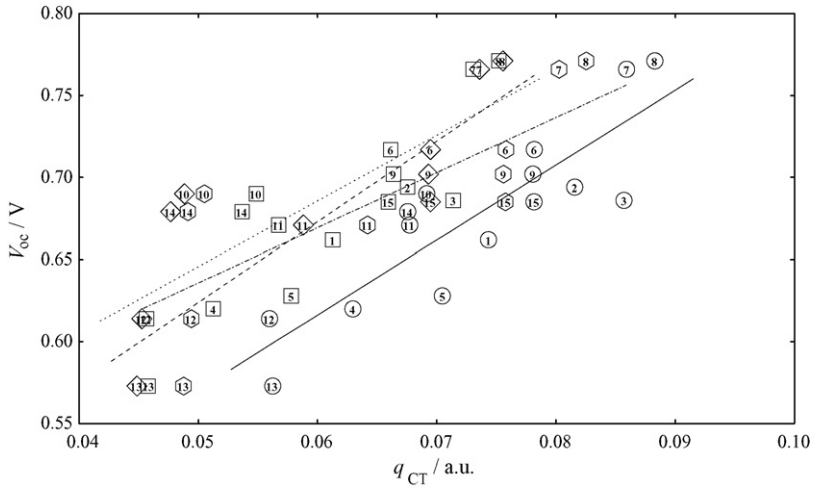

Fig. 5. Correlation between the V_{oc} of the cell and the net charge transferred (q_{CT}). (◯) Mulliken population analyses of complexes Py, (⬡) Mulliken population analyses of complexes A, (□) NBO analyses of complexes Py, (◇) NBO analyses of complexes A. Table 1 defines the number of each pyrazole.

favorable than **14**(*sp*) and **15**(*ap*), respectively. Consequently, various correlations between the V_{oc} values and the theoretical calculations of the intermolecular complexes were found. Fig. 3 represents the correlation between the V_{oc} of the cell and the intramolecular I–I and intermolecular N···I bond lengths in the complexes. Regardless of the binding site, as the I–I bond length becomes longer and becomes further from the isolated I_2 molecule one (2.694 Å), the V_{oc} value increases. The correlation coefficients are very high, and 0.864 for complexes Py (full line) and 0.825 for complexes A (dashed–dotted line). On the other hand, the shorter N···I bond length, the higher the V_{oc} value is. These correlation coefficients are also very high, −0.870 for complexes Py (dashed line) and −0.813 for complexes A (dotted line).

Fig. 4 depicts the correlation between the V_{oc} of the cell and the CP-corrected intermolecular bond energy (ΔE_b^{CP}). The larger the ΔE_b^{CP}, the higher the V_{oc} value is. The correlation coefficients are 0.577 for complexes Py (full line) and 0.784 for complexes A (dashed–dotted line).

Fig. 5 illustrates the correlation between the V_{oc} of the cell and the net charge transferred (q_{CT}) obtained from the Mulliken population analyses and NBO analyses. Regardless of the analytical method, the V_{oc} value becomes higher as q_{CT} increases. The correlation coefficients between the V_{oc} and q_{CT} determined by Mulliken population analyses are 0.870 for complexes Py (full line) and 0.795 for complexes A (dashed–dotted line), while those between the V_{oc} and q_{CT} determined by NBO analyses are 0.868 for complexes Py (dashed line) and 0.829 for complexes A (dotted line).

Fig. 6 shows the correlation of the V_{oc} with the occupancies of σ^*(I–I) and n_σ(N). These results indicate that the V_{oc} increases with the occupancies of σ^*(I–I) and generally decreases with that of n_σ(N). The correlation coefficients between the V_{oc} and σ^*(I–I) are 0.822 for complexes Py (full line) and 0.861 for complexes A (dashed–dotted line), while the correlation coefficients between the V_{oc} and n_σ(N) are −0.844 for complexes Py (dashed line) and −0.123 for complexes A (dotted line). Except for the correlation coef-

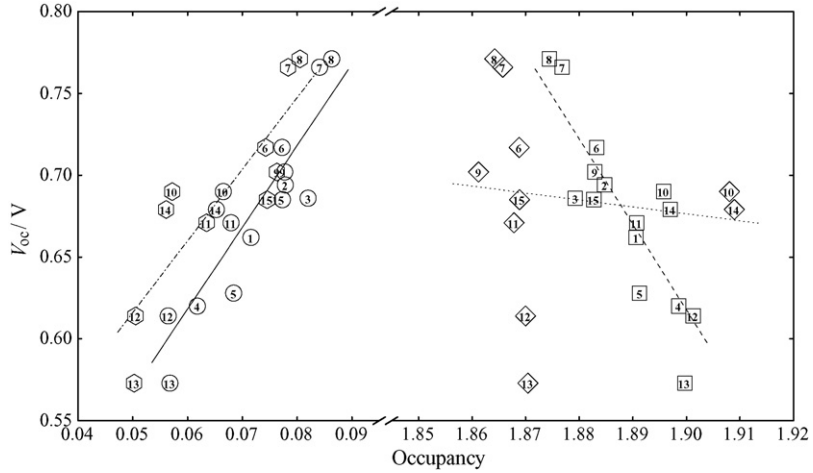

Fig. 6. Correlation between the V_{oc} of the cell and the occupancy. (◯) σ^*(I–I) occupancy of complexes Py, (⬡) σ^*(I–I) occupancy of complexes A, (□) n_σ(N) occupancy of complexes Py, (◇) n_σ(N) occupancy of complexes A. Table 1 defines the number of each pyrazole.

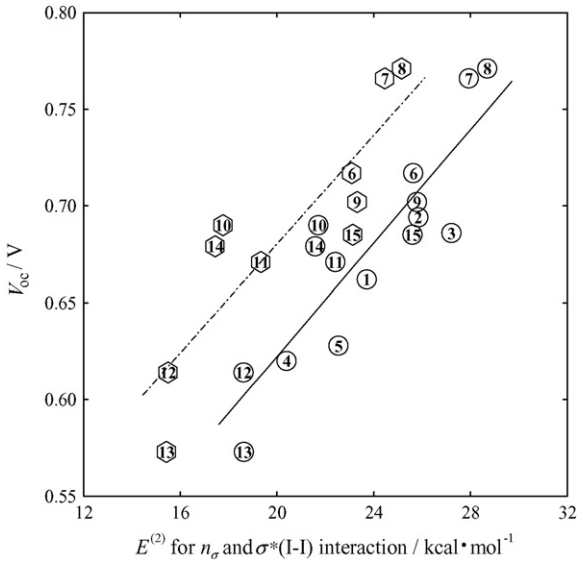

Fig. 7. Correlation between the V_{oc} of the cell and the second-order perturbation energy ($E^{(2)}$) for n_σ and σ^*(I—I) interaction. (◯) $E^{(2)}$ of complexes Py, (⬡) $E^{(2)}$ of complexes A. Table 1 defines the number of each pyrazole.

ficient for n_σ(N) of complexes A, these values are very high.

Fig. 7 depicts the correlation between the V_{oc} of the cell and $E^{(2)}$ for the n_σ(N) and σ^*(I–I) interaction in the complexes. The higher the $E^{(2)}$ value, the larger the V_{oc} of the solar cell. The correlation coefficients are very high, 0.880 for complexes Py (full line) and 0.874 for complexes A (dashed–dotted line).

All the correlations in Figs. 3–7 strongly suggest that a higher V_{oc} is obtained when I_2 and pyrazole complexes form a more favorable intermolecular charge-transfer complex. The chemical reactions of intermolecular donor–acceptor complexation in the I^-/I_3^- solution can be written as Eq. (5) [43]:

$$\text{Pyrazoles} + I_3^- \leftrightarrows \text{Pyrazoles–}I_2 + I^-. \quad (5)$$

This reaction decreases the I_3^- concentration, $[I_3^-]$, but increases the I^- concentration, $[I^-]$, which enhances the hole collection by I^- [44,45] and improves the V_{oc} value. Reducing the $[I_3^-]$ may also decrease the reaction between the injected electrons and I_3^- at the semiconductor electrolyte junction (Eq. (6) [45]), i.e. recombination,

$$I_3^- + 2e_{cb}^-(TiO_2) \xrightarrow{k_{et}[I_3^-]} 3I^-. \quad (6)$$

These changes would increase the electron concentration in the TiO_2 film and enhance the V_{oc} value (Eq. (7)) [2,46],

$$V_{oc} = \left(\frac{kT}{e}\right) \ln\left(\frac{I_{inj}}{n_{cb}k_{et}[I_3^-]}\right), \quad (7)$$

where k is the Boltzmann constant, T the absolute temperature, I_{inj} the charge flux that results from the sensitizing dye injecting an electron, n_{cb} the concentration of electrons at the TiO_2 surface, and k_{et} is the rate constant for I_3^- reduction by the conduction band electrons. In Eq. (7), the V_{oc} increases as the $[I_3^-]$ and/or k_{et} decreases [2,43]. Thus, the more intermolecular charge-transfer complexation and the lower the $[I_3^-]$, the more efficiently the holes are collected and/or the electron concentration in the TiO_2 film increases because the recombination reaction is prevented, which results in a higher V_{oc}.

Moreover, complexation of I_2 with pyrazoles may suppress the loss of the thiocyanato ligand (NCS^-) by I_3^- [43]:

$$(dcbpy)_2Ru(NCS)_2^{2-} + 2I_3^- \leftrightarrows (dcbpy)_2RuI_2^{2-} + 2I_2NCS^-. \quad (8)$$

Eq. (5) will cause equilibrium (8) to move to the left. The NCS ligand of the dye is believed to be important in the reduction of the oxidized dye to regenerate the original N719 dye. Rensmo et al. have confirmed by photoelectron spectroscopy experiments that both Ru(4d) and the atomic orbitals centered on the NCS ligands, in particular S(3p) wave functions, contribute to the frontier orbitals of the complex. The NCS ligands that point in the direction of the electrolyte may facilitate reduction of the oxidized dye by I^- [47]. This hypothesis is consistent with the result of Shi et al. [7] as mentioned in Section 1.

Therefore, the theoretical calculations confirm that the intermolecular donor–acceptor interactions between the I_2 and pyrazoles greatly influence the V_{oc} value in a Ru-dye-sensitized nanocrystalline TiO_2 solar cell with an I^-/I_3^- redox electrolytic solution.

5. Conclusions

This study investigated the charge-transfer 1:1 n–σ^* complexes of I_2 with 15 types of pyrazoles by the ab initio MO method with optimized geometries at the MP2(full)/LANL2DZ* level. The nitrogen atom at position 2 in the pyrazole ring and the amino nitrogen atom of the substituent are the preferred binding sites for I_2 molecules. Comparing complexes binding with I_2 via the nitrogen atom at position 2 in the pyrazole ring, the more electron donicity the substituent at positions 3 and 5 in the pyrazole ring, the more stable the intermolecular charge-transfer complex formed. However, pyrazoles with an electron-accepting substituent at position 4 form less favorable complexes with I_2 even if they are substituted by electron-donating group at positions 3 and/or 5.

These pyrazoles were also examined as additives in an I^-/I_3^- electrolyte solution on N719 dye-sensitized solar cell, and the resulted V_{oc} values were correlated with the intermolecular charge-transfer properties of complexes Py and A elucidated by theoretical calculations. A higher V_{oc} occurs when the energy of the pyrazoles HOMO level is close to the energy of the I_2 LUMO level. As the I–I bond length grows longer and becomes further from the isolated I_2 molecule length, the V_{oc} value increases. On the other hand, the shorter N···I bond length, the higher the V_{oc} value is. The larger the ΔE_b^{CP}, the more the V_{oc} value is. As q_{CT} increases, the V_{oc} value becomes higher. The value of V_{oc} increases with the occupancies of σ^*(I–I) and generally decreases with that of n_σ(N). The higher the $E^{(2)}$ value for the n_σ(N) and σ^*(I–I) interaction, the larger the V_{oc} of the solar cell. All these correlations strongly suggest that a higher V_{oc} is obtained when the I_2 and pyrazoles form a more favorable intermolecular charge-transfer complex

in the I^-/I_3^- redox electrolytic solution of dye-sensitized solar cell.

References

[1] B. O'Reganoulos, B.M. Grätzel, Nature 353 (1991) 737–740.
[2] S.Y. Huang, G. Schlichthörl, A.J. Nozik, M. Grätzel, A.J. Frank, J. Phys. Chem. B 101 (1997) 2576–2582.
[3] G. Schlichthörl, S.Y. Huang, J. Sprague, A.J. Frank, J. Phys. Chem. B 101 (1997) 8141–8155.
[4] G. Boschloo, H. Lindström, E. Magnusson, A. Holmberg, A. Hagfeldt, J. Photochem. Photobiol. A: Chem. 148 (2002) 11–15.
[5] G. Boschloo, A. Hagfeldt, Chem. Phys. Lett. 370 (2003) 381–386.
[6] H. Kusama, M. Kurashige, H. Arakawa, J. Photochem. Photobiol. A: Chem. 169 (2005) 169–176.
[7] C.W. Shi, S.Y. Dai, K.J. Wang, X. Pan, F.T. Kong, L.H. Hu, Vib. Spectrosc. 39 (2005) 99–105.
[8] C. Reid, R.S. Mulliken, J. Am. Chem. Soc. 76 (1954) 3869–3874.
[9] E.K. Plyler, R.S. Mulliken, J. Am. Chem. Soc. 81 (1959) 823–826.
[10] I. Haque, J.L. Wood, Spectrochim. Acta 23A (1967) 959–967.
[11] R.S. Mulliken, J. Am. Chem. Soc. 91 (1969) 1237.
[12] S. Aronson, P. Epstein, D.B. Aronson, G. Wieder, J. Phys. Chem. 86 (1982) 1035–1037.
[13] G. Maes, J. Mol. Struct. 61 (1980) 95–100.
[14] C.F. Merlevede, G. Maes, Adv. Mol. Relaxation Interact. Processes 16 (1980) 111–130.
[15] S.G. Ma, G.Z. Wu, J. Mol. Struct. 372 (1995) 127–130.
[16] M.J. El Ghomari, R. Mokhlisse, C. Laurence, J.Y. Le Questel, M. Berthelot, J. Phys. Org. Chem. 10 (1997) 669–674.
[17] M.M.A. Hamed, E.M. Abdalla, Sh.M. Bayoumi, Spectrosc. Lett. 36 (2003) 357–373.
[18] G.A. Bowmaker, P.D.W. Boyd, J. Chem. Soc. Faraday Trans. 2 (83) (1987) 2211–2223.
[19] Y. Zhang, C.Y. Zhao, X.Z. You, J. Phys. Chem. A 101 (1997) 2879–2885.
[20] Y. Zhang, X.-Z. You, J. Comput. Chem. 22 (2001) 327–338.
[21] Y. Danten, B. Guillot, Y. Guissani, J. Chem. Phys. 96 (1992) 3795–3810.
[22] S. Reilling, M. Besnard, P.A. Bopp, J. Phys. Chem. A 101 (1997) 4409–4415.
[23] M.J. Frisch, G.W. Trucks, H.B. Schlegel, G.E. Scuseria, M.A. Robb, J.R. Cheeseman, J.A. Montgomery Jr., T. Vreven, K.N. Kudin, J.C. Burant, J.M. Millam, S.S. Iyengar, J. Tomasi, V. Barone, B. Mennucci, M. Cossi, G. Scalmani, N. Rega, G.A. Petersson, H. Nakatsuji, M. Hada, M. Ehara, K. Toyota, R. Fukuda, J. Hasegawa, M. Ishida, T. Nakajima, Y. Honda, O. Kitao, H. Nakai, M. Klene, X. Li, J.E. Knox, H.P. Hratchian, J.B. Cross, V. Bakken, C. Adamo, J. Jaramillo, R. Gomperts, R.E. Stratmann, O. Yazyev, A.J. Austin, R. Cammi, C. Pomelli, J.W. Ochterski, P.Y. Ayala, K. Morokuma, G.A. Voth, P. Salvador, J.J. Dannenberg, V.G. Zakrzewski, S. Dapprich, A.D. Daniels, M.C. Strain, O. Farkas, D.K. Malick, A.D. Rabuck, K. Raghavachari, J.B. Foresman, J.V. Ortiz, Q. Cui, A.G. Baboul, S. Clifford, J. Cioslowski, B.B. Stefanov, G. Liu, A. Liashenko, P. Piskorz, I. Komaromi, R.L. Martin, D.J. Fox, T. Keith, M.A. Al-Laham, C.Y. Peng, A. Nanayakkara, M. Challacombe, P.M.W. Gill, B. Johnson, W. Chen, M.W. Wong, C. Gonzalez, J.A. Pople, Gaussian 03, Revision D.01, Gaussian Inc., Wallingford, CT, 2004.
[24] R. Dennington II, T. Keith, J. Millam, K. Eppinnett, W.L. Hovell, R. Gilliland, GaussView, Version 3.09, Semichem Inc., Shawnee Mission, KS, 2003.
[25] T.H. Dunning Jr., P.J. Hay, in: H.F. Schaefer III (Ed.), Modern Theoretical Chemistry, vol. 3, Plenum, New York, 1976, pp. 1–28.
[26] P.J. Hay, W.R. Wadt, J. Chem. Phys. 82 (1985) 270–283.
[27] W.R. Wadt, P.J. Hay, J. Chem. Phys. 82 (1985) 284–298.
[28] P.J. Hay, W.R. Wadt, J. Chem. Phys. 82 (1985) 299–310.
[29] M.W. Wong, P.M.W. Gill, R.H. Nobes, L. Radom, J. Phys. Chem. 92 (1988) 4875–4880.
[30] A.E. Reed, L.A. Curtiss, F. Weinhold, Chem. Rev. 88 (1988) 899–926.
[31] W. Schneider, W. Thiel, J. Chem. Phys. 86 (1987) 923–936.
[32] E. Cancès, B. Mennucci, J. Tomasi, J. Chem. Phys. 107 (1997) 3032–3041.
[33] M. Esseffar, W. Bouab, A. Lamsabhi, J.L.M. Abboud, R. Notario, M. Yáñez, J. Am. Chem. Soc. 122 (2000) 2300–2308.
[34] A. El Firdoussi, M. Esseffar, W. Bouab, J.-L.M. Abboud, O. Mó, M. Yáñez, J. Phys. Chem. A 108 (2004) 10568–10577.
[35] S.F. Boys, F. Bernardi, Mol. Phys. 100 (2002) 65–73.
[36] S. Simon, M. Duran, J.J. Dannenberg, J. Chem. Phys. 105 (1996) 11024–11031.
[37] S.P. Ananthavel, M. Manoharan, Chem. Phys. 269 (2001) 49–57.
[38] J.P. Foster, F. Weinhold, J. Am. Chem. Soc. 102 (1980) 7211–7218.
[39] E.D. Glendening, A.E. Reed, J.E. Carpenter, F. Weinhold, NBO Version 3.1.
[40] S.S.C. Ammal, S.P. Ananthavel, J. Chandrasekhar, P. Venuvanalingam, M.S. Hegde, Chem. Phys. Lett. 248 (1996) 153–157.
[41] A. Ebrahimi, F. Deyhimi, H. Roohi, J. Mol. Struct. (Theochem) 626 (2003) 223–229.
[42] K. Ohno, Ryoshi Butsuri Kagaku, University of Tokyo Press, Tokyo, 1989, pp. 311–312.
[43] H. Greijer, J. Lindgren, A. Hagfeldt, J. Phys. Chem. B 105 (2001) 6314–6320.
[44] M. Grätzel, Nature 414 (2001) 338–344.
[45] J. He, G. Benkö, F. Korodi, T. Polívka, R. Lomoth, B. Åkermark, L. Sun, A. Hagfeldt, V. Sundström, J. Am. Chem. Soc. 124 (2002) 4922–4932.
[46] M.K. Nazeeruddin, A. Kay, I. Rodicio, R. Humphry-Baker, E. Muller, P. Liska, N. Vlachopoulos, M. Grätzel, J. Am. Chem. Soc. 115 (1993) 6382–6390.
[47] H. Rensmo, S. Södergen, L. Patthey, K. Westermark, L. Vayssieres, O. Kohle, P.A. Brühwiler, A. Hagfeldt, H. Siegbahn, Chem. Phys. Lett. 274 (1997) 51–57.